Fractal and cumulative trace analysis of wire-line logs from a well in a naturally fractured limestone reservoir in the Gulf of Mexico

Rubén Darío Arizabalo[1], Klavdia Oleschko[2], Gabor Korvin[3], Gerardo Ronquillo[1] and Esteban Cedillo-Pardo[1]

[1] *Instituto Mexicano del Petróleo, Eje Central 152, Mexico City, Mexico*
[2] *Instituto de Geología, Universidad Nacional Autónoma de México, Mexico*
[3] *King Fahd University, Saudi Arabia*

RESUMEN

Hemos demostrado que los registros de pozo medidos en un yacimiento carbonatado naturalmente fracturado tienen un carácter fractal, estando sus parámetros fractales correlacionados con las propiedades petrofísicas de los depósitos. Los registros de porosidad neutrón, densidad, rayos gamma, tiempo de tránsito de la onda P y resistividad somera y profunda, se relacionaron bien con cinco estratos: Jurásico Superior Tithoniano y Kimmeridgiano (JST, JSK), Cretácico Superior, Medio e Inferior (KS, KM, KI). Cada una de estas capas tiene dimensiones fractales diferentes. Utilizando el software BENOIT se ajustaron las trazas de los registros como movimientos Brownianos fraccionarios (fBm) obteniéndose dimensiones fractales promedio para el registro de porosidad D=1.70 (KS), D=1.66 (KM), D=1.75 (KI), D=1.84 (JST), D=1.67 (JSK). Establecemos que la geometría fractal de los poros controla las fluctuaciones y dimensiones fractales de los registros en cada unidad geológica. El análisis de las trazas acumuladas ha proporcionado una mejor comprensión del sistema, incluyendo las cinco unidades principales.

PALABRAS CLAVE: Fractales estadísticos, registros geofísicos de pozo, yacimiento naturalmente fracturado, Golfo de México.

ABSTRACT

We found that the wire-line well logs measured in a naturally fractured limestone reservoir show fractal behavior, and that the fractal parameters are correlated with the petrophysical properties. Based on neutron porosity, bulk density, gamma ray, P-wave transit time, shallow and deep resistivity logs, five strata were distinguished corresponding to the Tithonian and Kimmeridgian Jurassic (JST, JSK); Upper, Middle and Lower Cretaceous (KS, KM, KI). Each of these strata has different fractal dimensions. Using the BENOIT software we obtained average fractal dimensions for the logs by modeling them as fractional Brownian motion (fBm). For the neutron porosity log D=1.70 (KS), D=1.66 (KM), D=1.75 (KI), D=1.84 (JST), D=1.67 (JSK). We conclude that the fractal geometry of the pore space controls the log fluctuations as well as the fractal dimensions of the logs in each geological unit. Cumulative trace analysis has provided further insight, including zonation of the five main units.

KEY WORDS: Statistical fractals, wire-line logs, naturally fractured reservoir, Gulf of Mexico.

INTRODUCTION

One way to understand geological patterns in space and time is given by fractal geometry (Mandelbrot, 1975, 1977, 1983). This geometry helps to quantify the spatial heterogeneities of different geological patterns, in a way that is useful in oil exploration and production (Barton and La Pointe, 1995). More recently, fractals have been applied to reservoir engineering for modeling rock property distributions based on scaling laws (Hardy and Beier, 1994).

The present work analyses the porosity distributions derived from neutron-, gamma-ray, and sonic travel-time logs from Cantarell oil field in the Gulf of Mexico. Hewett (1986) noticed the fractal behavior of porosity well logs. He ob-tained the fractal dimension using rescaled range (R/S) analysis (Feder, 1988; Korvin, 1992), a method originally proposed by Hurst (1965). Hardy (1992) and Crane and Tubman (1990) also modeled reservoir variability with fractals.

METHODOLOGY

We carried out fractal analysis of neutron porosity (NPHI) (Figure 1), bulk density (RHOB), P wave transit time (DT), gamma ray (GR), shallow laterolog (LLS), and deep laterolog (LLD) resistivity well logs. A total number of 29 traces for one well were analyzed, the depth range studied includes five layers: Upper, Middle and Lower Cretaceous (KS, KM, KI), and Tithonian and Kimmeridgian Jurassic (JST, JSK), in a hydrocarbon-containing naturally fractured
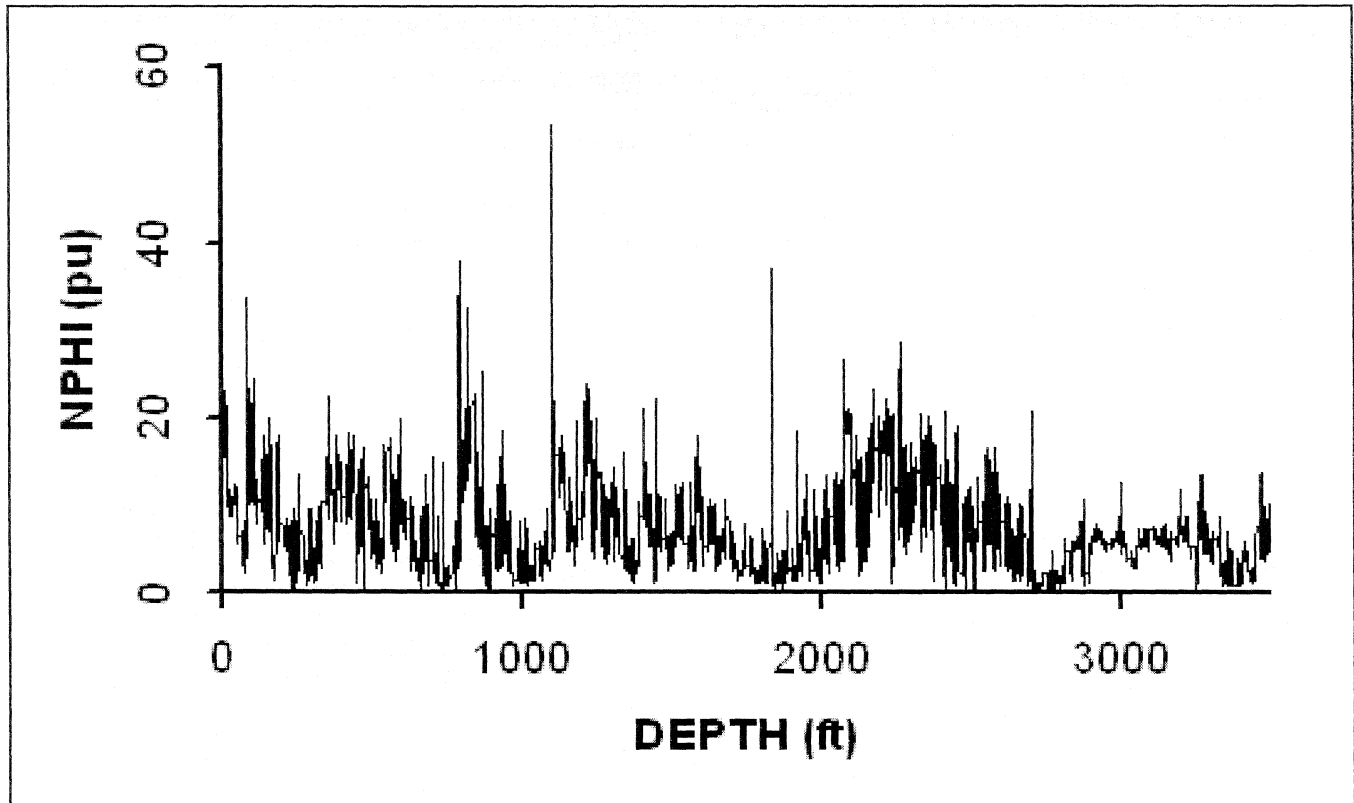
Fig. 1. NPHI log for the study interval, including Cretaceous and Jurassic strata.

limestone reservoir in Cantarell oil field, Gulf of Mexico. From this well, cores and plugs were also selected for fractal image analyses, not reported here.

In the study area, dolomitized limestones and dolomites of the Kimmeridgian, limestones and breccias of the Cretaceous, as well as calcareous breccias at the base of the Paleocene, constitute the reservoir rocks. According to the wire-line logs and core data, Paleocene breccias represent the reservoirs, Jurassic rocks, mainly of the Tithonian, provide the source rocks. The best HC accumulations can be observed in anticlines with faults located in a strip subjected to fractures and advanced diagenesis. Paleocene breccias, dolomites and fractured limestones from the Cretaceous and Jurassic, have an oil-saturated total thickness of hundreds of meters. In Cantarell oil field, such rocks can be found at depths 1200 m to 3000 m (Santiago-Acevedo *et al.*, 1984.)

In this study wire-line logs are considered as self-affine fractals. Unlike self-similar fractals, which scale similarly in the *x* and *y* directions, a self-affine fractal must be scaled by different factors in different coordinate directions. For example, if the scaling factor is λ_x in the x-coordinate, and λ_y in the y-coordinate, then

$$\lambda_x = \lambda \tag{1}$$

$$\lambda_y = \lambda^H \tag{2}$$

$$H = \log(\lambda_y)/\log(\lambda_x) , \tag{3}$$

where H is the Hurst exponent. For example, if $\lambda_x = 3, \lambda_y = 2$,

$$H = \log 2/\log 3 = 0.631. \tag{4}$$

Fractional Brownian motion

Fractional Brownian motion (fBm) is a non-stationary self-affine random process, defined by Mandelbrot and Van Ness (1968) as

$$B_H(t) = \frac{1}{\Gamma(H+0.5)} \left\{ \int_{-\infty}^{0} \left[|t - \ell|^{H-0.5} - |\ell|^{H-0.5} \right] dB(\ell) + \int_{0}^{t} |t - \ell|^{H-0.5} dB(\ell) \right\} \tag{5}$$

where $\Gamma(x)$ is the gamma function, and B(t) an ordinary Gaussian process with zero mean and unit variance. Self-affinity implies that

$$B_H(\lambda t) - B_H(0) = \lambda^H \{B_H(t) - B_H(0)\}. \qquad (6)$$

The parameter H is the Hurst coefficient ($0 < H < 1$), related to the Hausdorff fractal dimension as $D = 2 - H$.

The auto-correlation function of a fBm is (Fortin *et al.*, 1992)

$$\rho_{B_H}(t, \ell) = \frac{1}{2} V_H \left\{ |t|^{2H} - |t - \ell|^{2H} + |\ell|^{2H} \right\}, \qquad (7)$$

where

$$V_H = \Gamma(1 - 2H) \frac{\cos(\pi H)}{\pi H}. \qquad (8)$$

Thus the time-averaged power spectral density (PSD) of a fBm is

$$S_{B_H} = \frac{1}{|f|^{2H+1}}. \qquad (9)$$

Fractional Gaussian noise

Fractional Gaussian noise (fGn) is a Gaussian stationary process derived from fBm by

$$Z(x) = \lim_{\delta \to 0} \frac{B_H(x + \delta) - B_H(x)}{\delta}. \qquad (10)$$

It has zero mean and its variance is

$$Var\left\{ \frac{B_H(x + \delta) - B_H(x)}{\delta} \right\} = V_H \, \delta^{2H-2}, \qquad (11)$$

where V_H is defined in Equation (8).

From the fBm autocorrelation, Equation (7), and using the definition of fGn, it is possible to evaluate the fGn's auto-correlation function (Hewett, 1986; Fortin *et al.*, 1992) and derive its power spectral density (PSD) as:

$$S_{Z_H} = \frac{1}{|f|^{2H-1}}. \qquad (12)$$

DETERMINATION OF THE HURST EXPONENT AND THE FRACTAL DIMENSIONS

The power spectral analysis routine in BENOIT (1999) for self-affine fractal traces yields the exponent $\beta = 2H + 1$ in

Equation (9). If $1 < \beta < 3$, we obtain the Hurst exponent H which, by Equation (6), characterizes the scale-dependent roughness of the trace. For exact, theoretical self affine curves a single fractal dimension, such as D=2-H would be sufficient to characterize the self affinity of the curve. For empirically observed traces however, the Hurst exponents computed in different ways are slightly different, and additional, generally different fractal dimensions can be introduced. (See Feder 1988, Korvin 1992. Most of these fractal dimensions can also be computed by the BENOIT software.) As we shall see later, only some of the possible fractal dimensions show meaningful correlation with the petrophysical geological features of the different well-log traces.

The Hurst exponent H can also be computed from rescaled range (R/S) analysis (Feder, 1988). Define the range R of a process as the difference between the maximum and minimum of the cumulative X values:

$$R(\ell) = \max_{1 \le t \le \ell} X(t, \ell) - \min_{1 \le t \le \ell} X(t, \ell) \ , \qquad (13)$$

where l is the period considered and t is an integer value of time. Define the dimensionless ratio R/S, called rescaled range, where S is the standard deviation,

$$S(\ell) = \left\{ \frac{1}{\ell} \sum_{t=1}^{\ell} [\xi_t - <\xi>]^2 \right\}^{1/2}. \qquad (14)$$

Then, the rescaled range grows with time as (Feder, 1988):

$$R(\ell)/S(\ell) = (\ell/2)^H. \qquad (15)$$

When $1 > H > 0.5$, the behavior is called persistent (that is the locally observed trend continues), while $0 < H < 0.5$ implies an antipersistent behavior.

Let $P(k)$ be the value of the power spectrum of a fractal process at some wavenumber ($k = 2\pi/\lambda$, where λ is wavelength). To estimate the fractal dimension one plots the logarithm of $P(k)$ versus the logarithm of k. A straight line with a negative slope $-b$ is expected if the trace is self-affine and the fractal dimension estimated from the power spectrum is

$$D_S = \frac{5 - b}{2}. \qquad (16)$$

The *Roughness-Length* method computes the root-mean-square (RMS) roughness of the data in windows of

size l. For a self-affine trace, the RMS roughness S(l) measured in a window of size l grows with window length l as

$$S(\ell) \approx \ell^H, \tag{17}$$

where H is the Hurst exponent. The fractal dimension D_{rl} estimated from this RMS roughness analysis is

$$D_{rl} = 2 - H. \tag{18}$$

A similar technique is based on the *Variogram Method*, where one computes the variogram, that is the expected value of the squared difference between two values in a trace z (t) separated by a distance l

$$2\gamma(\ell) = E\left\{ [z(t) - z(t + \ell)]^2 \right\}. \tag{19}$$

(Geostatisticians use γ (l), the so-called "semivariogram" - see Goovaerts, 1997 - and l, the distance of separation, is referred to as the "lag".) For a self-affine trace, and for small values of l, from Equation 17 one gets:

$$2\gamma(\ell) \approx \ell^{2H} \tag{20}$$

and the fractal dimension D_v estimated from the variogram is obtained as $D_v = 2 - H$.

The *wavelets method* is based on wavelet analysis (Burrus *et al.*, 1998). The self-affine trace is decomposed in time- frequency space in such a manner that the variability both in time and frequency can be determined. If the wavelet power spectrum is a power-law function of frequency, this indicates fractal properties. The BENOIT program contains an heuristically defined function f which establishes an approximate relation between the Hurst exponent H and G_{avg} in the form $H = f(G_{avg})$ for stochastic self-affine traces. Finally, the wavelet fractal dimension is obtained as $D_w = 2 - H$.

RESULTS OF THE FRACTAL ANALYSIS

Table 1 shows the Hurst exponent (H) and fractal dimension (D) of well logs for the relevant lithologies, obtained by rescaled range (D_{rs}), power spectra (D_s), roughness-length (D_{rl}), variogram (D_v) and wavelets (D_w) methods. Data are presented for the following logs: neutron porosity (NPHI), bulk density (RHOB), sonic travel-time (DT), sonic velocity (1/DT), natural gamma ray (GR), shallow laterolog (LLS), and deep laterolog (LLD). In order to simplify the analysis, we decided to use for comparison the average value of the five different fractal dimensions, that is

$$D_{avr} = \frac{1}{5}\left\{ D_{rs} + D_s + D_{rl} + D_v + D_w \right\}.$$

For the NPHI log, average dimensions estimated for the different formations are 1.71 (KS), 1.68 (KM), 1.79 (KI), 1.88 (JST), and 1.75 (JSK). The average NPHI values in percent for the same strata are 8.6 (KS), 7.2 (KM), 7.4 (KI), 9.6 (JST), and 5.0 (JSK).

Figure 2 shows the correlation between average fractal dimension D_{avr} and average neutron porosity ϕ_{avr}. A fair positive correlation was obtained with coefficient of correlation 0.45 which has become notably better (0.72) when the variogram- and wavelet dimensions were excluded from analysis (Table 2 a, b). Leaving out D_v and D_w, the average fractal dimensions become: 1.70 (KS), 1.66 (KM), 1.75 (KI), 1.84 (JST), 1.67 (JSK), showing (Figure 3) improved correlation between ϕ_{avr} and the average of the dimensions D_{avr}, D_{rs}, D_s, and D_r.

Table 2-c and Figure 4 show negative correlation between average fractal dimension and bulk density (RHOB) (-0.25). This means D_{avr} increases when RHOB decreases, and inversely. By the well-known relation between bulk density and porosity

$$\rho_{bulk} = \Phi\rho_{fluid} + (1 - \Phi)\rho_{grain} \tag{22}$$

(Mavko *et al.*, 1998 p. 251) for fluid-filled sedimentary rocks, where RHO$_{fluid}$ $\approx$ 1 g/cm^3 and RHO$_{grain}$ can be assumed constant (2.5-2.7 g/cm^3) in our limited depth range, Equation (22) implies that RHOB and ϕ are inversely related, and the negative correlation between RHOB and D_{avr} corresponds to a positive correlation between D_{avr} and porosity, as in the previous case, if we assume that neutron porosity NPHI and total porosity ϕ are proportional.

Table 2-d and Figure 5 show no correlation between the average fractal dimension and gamma ray log (0.1). Be-
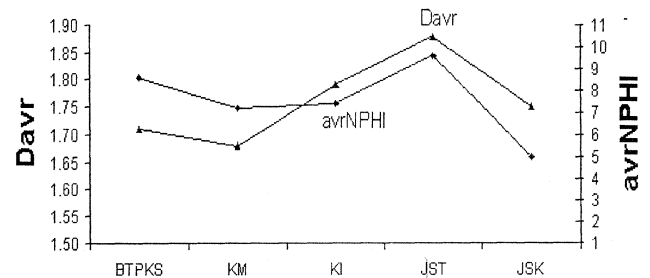

Fig. 2. Comparison of the average fractal dimension of porosity obtained from the five fractal analysis methods (D_{avr}) with the average total porosity of the NPHI log for each geological unit.

Table 1

Estimation of Hurst coefficient (H) and fractal dimension (D) from well log data from a well in the Gulf of Mexico

Well Log	Analysis	BTPKS H (D)	KM H (D)	KI H (D)	JST H (D)	JSK H (D)
NPHI	R/S	0.327 (1.673)	0.264 (1.736)	0.275 (1.725)	0.201 (1.799)	0.340 (1.660)
	Power spectra	0.324 (1.676)	0.385 (1.615)	0.232 (1.768)	0.150 (1.850)	0.376 (1.624)
	Roughness-L	0.247 (1.753)	0.383 (1.617)	0.255 (1.745)	0.124 (1.876)	0.268 (1.732)
	Variogram	0.166 (1.834)	0.139 (1.861)	0.084 (1.916)	0.121 (1.879)	0.139 (1.861)
	Wavelets	0.369 (1.631)	0.442 (1.558)	0.219 (1.781)	0.005 (1.995)	0.131 (1.869)
RHOB	R/S	0.296 (1.704)	0.228 (1.772)	0.262 (1.738)	0.252 (1.748)	0.274 (1.726)
	Power spectra	0.248 (1.752)	0.176 (1.824)	0.165 (1.835)	0.135 (1.865)	0.322 (1.678)
	Roughness-L	0.213 (1.787)	0.326 (1.674)	0.182 (1.818)	0.101 (1.899)	0.181 (1.819)
	Variogram	0.098 (1.902)	0.121 (1.879)	0.050 (1.950)	0.030 (1.970)	0.086 (1.914)
	Wavelets	0.238 (1.762)	0.399 (1.601)	0.069 (1.931)	0.132 (1.868)	0.036 (1.964)
DT	R/S				0.184 (1.816)	0.256 (1.744)
	Power spectra				0.265 (1.735)	0.055 (1.945)
	Roughness-L				0.176 (1.824)	0.160 (1.840)
	Variogram				0.153 (1.847)	0.143 (1.857)
	Wavelets				0.419 (1.581)	0.072 (1.928)
1/DT	R/S				0.191 (1.809)	0.249 (1.751)
	Power spectra				0.245 (1.755)	0.056 (1.944)
	Roughness-L				0.170 (1.830)	0.166 (1.834)
	Variogram				0.128 (1.872)	0.155 (1.845)
	Wavelets				0.426 (1.574)	0.081 (1.919)
GR	R/S	0.281 (1.719)	0.214 (1.786)	0.289 (1.711)	0.147 (1.853)	0.311 (1.689)
	Power spectra	0.218 (1.782)	0.086 (1.914)	0.033 (1.967)	0.035 (1.965)	0.224 (1.776)
	Roughness-L	0.193 (1.807)	0.291 (1.709)	0.184 (1.816)	0.088 (1.912)	0.233 (1.767)
	Variogram	0.154 (1.846)	0.139 (1.861)	0.033 (1.967)	0.090 (1.910)	0.196 (1.804)
	Wavelets	0.113 (1.887)	0.232 (1.768)	0.054 (1.946)	0.184 (1.816)	0.230 (1.770)
LLS	R/S	0.389 (1.611)	0.327 (1.673)	0.275 (1.725)	0.273 (1.727)	0.567 (1.433)
	Power spectra	0.330 (1.670)	0.436 (1.564)	0.226 (1.774)	0.397 (1.603)	0.421 (1.579)
	Roughness-L	0.298 (1.702)	0.399 (1.601)	0.341 (1.659)	0.292 (1.708)	0.380 (1.620)
	Variogram	0.226 (1.774)	0.306 (1.694)	0.137 (1.863)	0.162 (1.838)	0.288 (1.712)
	Wavelets	0.395 (1.605)	0.474 (1.526)	0.489 (1.511)	0.491 (1.509)	0.514 (1.486)
LLD	R/S	0.381 (1.619)	0.328 (1.672)	0.241 (1.759)	0.302 (1.698)	0.438 (1.562)
	Power spectra	0.000 (2.000)	0.000 (2.000)	0.000 (2.000)	0.000 (2.000)	0.281 (1.719)
	Roughness-L	0.335 (1.665)	0.352 (1.648)	0.319 (1.681)	0.079 (1.921)	0.450 (1.550)
	Variogram	0.056 (1.944)	0.039 (1.961)	-0.007	0.008 (1.992)	0.250 (1.750)
	Wavelets	0.170 (1.830)	0.161 (1.839)	0.268 (1.732)	0.004 (1.996)	0.616 (1.384)

Table 2

Correlation coefficients of fractal dimensions from several analysis methods (R/S, power spectrum, roughness-length, variogram and wavelets) and average values of porosity, density, gamma ray, shallow and deep resistivity

		D_{avr}	ϕ_{avr}	Drs	Ds	Dr	Dv	Dw
	D_{avr}	1.00						
	ϕ_{avr}	0.45	1.00					
	Drs	0.65	0.68	1.00				
a)	Ds	0.92	0.71	0.74	1.00			
	Dr	0.90	0.56	0.43	0.85	1.00		
	Dv	0.54	-0.00	0.45	0.56	0.19	1.00	
	Dw	0.91	0.11	0.38	0.68	0.84	0.40	1.00

		D_{avr}	ϕ_{avr}	Drs	Ds	Dr	Dv	Dw
	D_{avr}	1.00						
	ϕ_{avr}	0.72	1.00					
b)	Drs	0.77	0.68	1.00				
	Ds	0.99	0.71	0.74	1.00			
	Dr	0.88	0.56	0.43	0.85	1.00		

		D_{avr}	avr.RHOB	Drs	Ds	Dr	Dv	Dw
	D_{avr}	1.00						
	avr.RHOB	-0.25	1.00					
	Drs	-0.11	0.23	1.00				
c)	Ds	0.29	-0.17	0.60	1.00			
	Dr	0.92	-0.53	-0.37	0.09	1.00		
	Dv	0.98	-0.34	-0.05	0.46	0.90	1.00	
	Dw	0.81	0.04	-0.45	-0.29	0.79	0.69	1.00

		D_{avr}	avr.GR	Drs	Ds	Dr	Dv	Dw
	D_{avr}	1.00						
	Avr.GR	0.10	1.00					
	Drs	0.54	0.59	1.00				
d)	Ds	0.84	0.14	0.62	1.00			
	Dr	0.75	0.48	0.47	0.37	1.00		
	Dv	0.91	-0.19	0.28	0.87	0.47	1.00	
	Dw	0.58	-0.62	-0.30	0.25	0.36	0.70	1.00

		D_{avr}	avr.LLS	Drs	Ds	Dr	Dv	Dw
	D_{avr}	1.00						
	avr.LLS	-0.61	1.00					
	Drs	0.83	-0.63	1.00				
e)	Ds	0.77	-0.52	0.41	1.00			
	Dr	0.71	-0.15	0.39	0.38	1.00		
	Dv	0.90	-0.21	0.64	0.76	0.72	1.00	
	Dw	0.35	-0.68	0.15	0.22	0.47	0.00	1.00

		D_{avr}	avr.LLD	Drs	Ds	Dr	Dv	Dw
	D_{avr}	1.00						
	avr.LLD	-0.60	1.00					
	Drs	0.78	-0.61	1.00				
f)	Ds	0.94	-0.83	0.74	1.00			
	Dr	0.83	-0.05	0.53	0.58	1.00		
	Dv	0.96	-0.77	0.87	0.97	0.65	1.00	
	Dw	0.96	-0.54	0.60	0.91	0.82	0.88	1.00

cause the natural gamma ray log represents total clay content and the analyzed carbonates are almost clay-free, the gamma log has no physical relation with porosity that controls D_{avr}.

Figure 6 and Table 2-e show negative correlation between $\log_{10}$(LLS) and average fractal dimension. This is due to the fact that if the fluid content does not change, resistivity depends on porosity as ~ $1/\phi^2$ (by Archie's law, Mavko *et al.*, 1998). Consequently, resistivity has negative correlation with porosity that is with D_{avr} as well. Finally, by Figure 7 and Table 2-f there is negative correlation between $\log_{10}$(LLD) and average fractal dimension (-0.6). The explanation is same as before.

The correlation between the average wire-line logs is poor, except between GR and LLS, GR and LLD, LLS and LLD (Table 3-a). The good correlation between LLS and LLD might be due to the fact that there had been no serious invasion of the drilling liquid into the formation. As for GR, its increase implies a larger amount of diagenetic clay minerals. These clay minerals block the path of the conducting electric charge-carriers. That is, if natural gamma increases, then clay minerals are more abundant, and resistivity also increases.

For all logs starting in KS, the average fractal dimension D_{avr} slightly falls (KM), then rises (KI), further rises (JST), and finally drops (JSK). Good correlation can be ob-

a)

b)

c)

Fig. 3a, b, c. Fractal dimensions of porosity obtained with R/S, power spectrum and roughness-length methods; and their comparison with the average NPHI log trend.
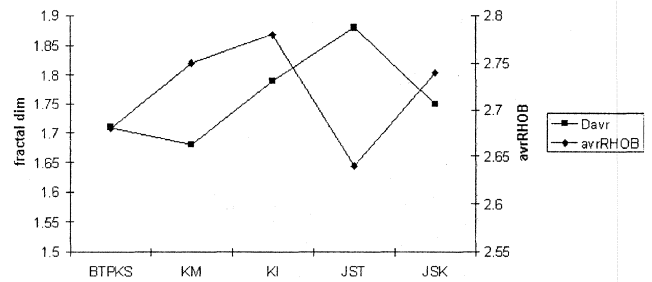

Fig. 4. Average densities [g /cm³] and average fractal dimensions of the porosity logs. They are almost mirror images of each other.
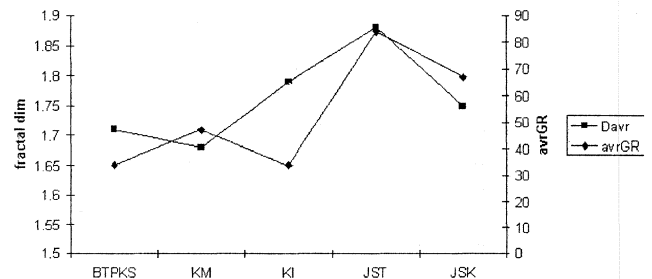

Fig. 5. The gamma ray log is not correlated with the average fractal dimension of the porosity log.
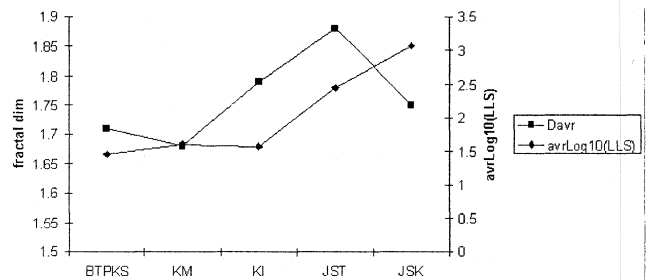

Fig. 6. Negative correlation between the average logarithmic values of close-to-borehole resistivity and average fractal dimension of the porosity log. Note the increase in resistivity in the Jurasssic.

Table 3

Average well log values for each lithology and their correlation coefficients

avr.NPHI	avr. RHOB	avr. GR	avr.log$_{10}$(LLS)	avr.log$_{10}$(LLD)	strata
8.6	2.68	34	1.46	2.48	KS
7.2	2.75	47	1.6	2.5	KM
7.4	2.78	34	1.57	2.39	KI
9.6	2.64	84	2.45	3.18	JST
5	2.74	67	3.07	3.7	JSK

	avr. PHI	avr. RHOB	avr. GR	avr.log$_{10}$(LLS)	avr.log10 (LLD)
avr. NPHI	1				
avr. RHOB	-0.7	1			
avr. GR	0.08	-0.56	1		
avr.log$_{10}$(LLS)	-0.45	-0.19	0.81	1	
avr.log$_{10}$(LLD)	-0.43	-0.25	0.8	0.99	1

a) applies to the second table above.

avr.dim.NPHI	avr.dim.RHOB	avr.dim.GR	avr.dim.LLS	avr.dim.LLD	strata
1.71+/-0.05	1.78+/-0.06	1.81+/-0.03	1.67+/-0.07	1.81+/-0.03	KS
1.68+/-0.05	1.75+/-0.03	1.8+/-0.02	1.61+/-0.02	1.82+/-0.02	KM
1.79+/-0.05	1.85+/-0.05	1.88+/-0.05	1.71+/-0.29	1.84+/-0.04	KI
1.88+/-0.03	1.87+/-0.05	1.89+/-0.04	1.68+/-0.07	1.92+/-0.02	JST
1.75+/-0.07	1.82+/-0.07	1.76+/-0.05	1.56+/-0.04	1.59+/-0.07	JSK

	avr.dim.NPHI	avr.dim.RHOB	avr.dim.GR	avr.dim.LLS	avr.dim. LLD
avr.dim.NPHI	1				
avr.dim.RHOB	0.95	1			
avr.dim.GR	0.74	0.67	1		
ave.dim.LLS	0.45	0.44	0.89	1	
avr.dim.LLD	0.41	0.22	0.85	0.82	1

b) applies to the fourth table above.

served between average fractal dimensions for neutron porosity and bulk density (0.95); and for neutron porosity and gamma ray (0.74). But there is poor correlation between average fractal dimensions for LLS (0.45) and LLD (0.41). The average fractal dimension for GR correlates with the average fractal dimension for RHOB (0.67), LLS (0.89), and LLD (0.85).

CUMULATIVE TRACE ANALYSIS

To understand the global behavior of well-logs in the five main formations, we constructed *cumulative traces* from each well logs. Introduced by Dolan *et al*. (1998), the cumu-
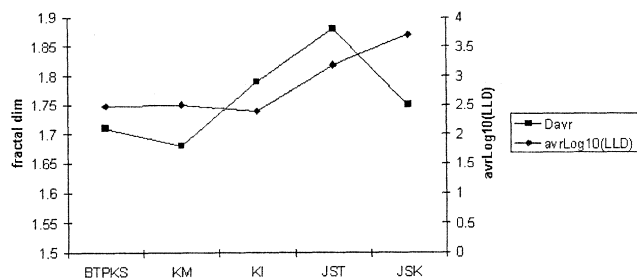

Fig. 7. As in the previous figure, the average "deep" resistivity logarithmic trend is opposite to the average porosity fractal dimension trend, notably in the Jurassic.

lative trace is defined as follows. Suppose a well log trace $f(z)$ is measured in the depth range $[Z_1, Z_2]$, and by a proper normalization and shift we assure that $\int_{Z_1}^{Z_2} f(z)dz = 0; \quad \int_{Z_1}^{Z_2} f^2(z)dz = 1.$

The cumulative trace $f_{cum}(Z) = \int_{Z_1}^{Z} f(z)dz; \quad z \in [Z_1, Z_2],$ reflects long-wavelength correlations or system "memory". Figure 8 shows such cumulative sums for neutron porosity, bulk density, gamma ray, shallow laterolog and deep laterolog well logs.

In KI (Figure 8) there are three distinctive zones. For the middle zone we have high porosity, low density, low gamma ray (no clay, i.e. good permeability) and high LLD. A question immediately arises, how can resistivity be high when porosity is high? Archie's law states that $\rho_{rock} = \rho_{fluid}/\Phi^2$. As ϕ is large, ρ_{fluid} must also be large to give a high rock bulk resistivity, implying that the pore-fluid is probably hydrocarbon rather than brine. For the Tithonian (Figure 9), we have two zones. The upper zone shows low gamma ray, low porosity, high P-wave velocity, high bulk density and high LLD, which indicates a low porosity non-productive carbonate. The lower zone shows low resistivity, low density, high porosity, a gamma-ray which is decreasing with depth, low P-velocity, and low LLD. The decreasing gamma ray with depth suggests that during deposition of this formation the sea level was decreasing. This zone is possibly brine-filled because of its low resistivity. Figure 10 indicates three main zones in JSK: the upper zone has high resistivity, high velocity, low density, low gamma ray, and low porosity, which suggests a non-reservoir clay-free low-porosity carbonate. The middle zone shows high gamma ray, high density, high velocity, low porosity and low resistivity: it is a clay-rich non-reservoir carbonate. The oldest zone represents low porosity, low gamma ray, medium LLD, and high P-velocity; so we have a non-reservoir carbonate. The low-to-medium LLD and small porosity might indicate intensive fracturing filled with brine. There is an unconformity (perhaps a good seismic reflector?) between the middle and lower zones.

CONCLUSIONS

From the analysis of the borehole data the following conclusions can be drawn:

1. The distinctly different petrophysical properties in the five main geological units are also associated with different fractal porosity-log models, with respective average fractal dimensions: D=1.70 (KS), D=1.66 (KM), D=1.75 (KI), D=1.84 (JST), D=1.67 (JSK).

2. The fractal (power-law) scaling which has been observed, is possibly due to the fractal distribution of pore space.
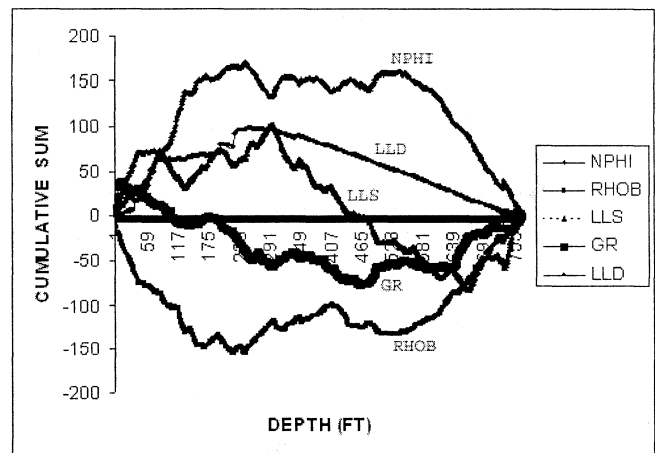

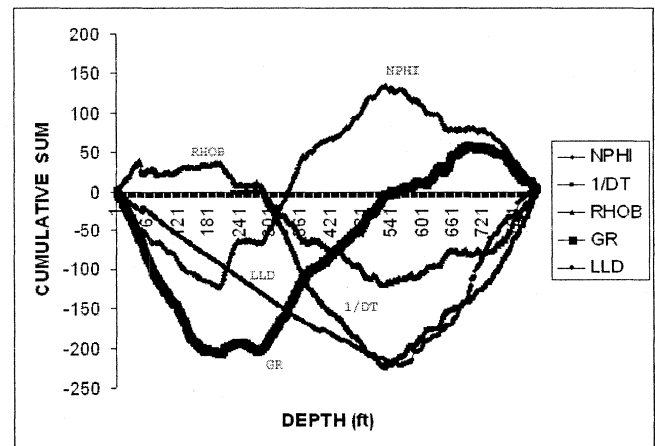Figure 8. Cumulative traces of porosity, density, gamma rays and resistivity for the Lower Cretaceous.

Fig. 9. Tithonian cumulative traces of porosity, P-wave velocity, gamma rays, density and resistivity.
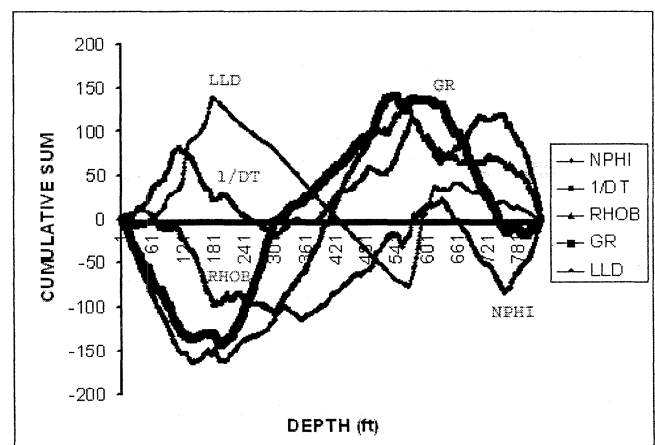

Figure 10. Cumulative behavior of porosity, P-wave velocity, density, gamma rays and deep resistivity in the Kimmeridgian.

3. The cumulative sums of the normalized logs suggest a productive zone in the KI and a seismic reflector in JSK.

ACKNOWLEDGMENTS

BIBLIOGRAPHY

BARTON, C. and P. R. LA POINTE, 1995. Fractals in Petroleum, Geology and Earth Processes. Plenum Press, New York.

BENOIT 1.2, 1999. http://www.trusoft.netmegs.com; Seffens, W., 1999. *Science, 285, 5431,* 1228.

BURRUS, C., R. GOPINATH and H. GUO, 1998. Introduction to Wavelets and Wavelet Transforms. Prentice Hall, New York.

CRANE, S. E. and K. T. TUBMAN, 1990. Reservoir variability and modeling with fractals. SPE Paper 20606, SPE Ann. Tech. Conf., New Orleans.

DOLAN, S. S., CH. J. BEAN and B. RIOLLET, 1998. The broad-band fractal nature of heterogeneity in the upper crust from petrophysical logs. *Geophys. J. Int. 132,* 489-507.

FEDER, J., 1988. Fractals. Plenum Press, NY. 283 pp.

FORTIN, C., R. KUMARESAN, W. OHLEY and S. HOEFER, 1992. Fractal Dimension in the Analysis of Medical Images. IEEE Eng. Med. Biol., Jun 1992. 65-71.

GOOVAERTS, P., 1997. Geostatistics for Natural Resources Evaluation. Oxford University Press, New York.

HARDY, H. H., 1992. The generation of reservoir property distributions in cross section for reservoir simulation based on core and outcrop photos. SPE Paper 23968, presented at SPE Permian Basin Oil and Gas Recovery Conf., Midland, Texas.

HARDY, H. H. and R. A. BEIER, 1994. Fractals in Reservoir Engineering. World Scientific. 359 pp.

HEWETT, T. A., 1986. Fractal distributions of reservoir heterogeneity and their influence on fluid transport. SPE Paper 15386, presented at SPE Ann. Tech. Conf., New Orleans.

HURST, H. E., R. P. BLACK and Y. M. SIMAIKA, 1965. Long-Term Storage: An experimental Study. Constable, London.

KORVIN, G., 1992. Fractal Models in the Earth Sciences. Elsevier, Amsterdam.

MANDELBROT, B. B. and J. W. VAN NESS, 1968. Fractional Brownian Motions, Fractional Noises and Applications. *SIAM Rev., 10, 4,* 422-437.

MANDELBROT, B. B., 1975. Les Objets Fractals: Forme, Hasard et Dimension. Flammarion, Paris.

MANDELBROT, B. B., 1977. Fractals: Form, Chance, and Dimension. W.H. Freeman and Co., San Francisco.

MANDELBROT, B. B., 1983. The Fractal Geometry of Nature. W.H. Freeman and Co., New York.

MAVKO, G., T. MUKERJI and J. DVORKIN, 1998. The Rock Physics Handbook. Tools for Seismic Analysis in Porous Media. Cambridge University Press, Cambridge, UK.

SANTIAGO-ACEVEDO, J., J. CARRILLO-BRAVO and B. MARTELL-ANDRADE, 1984. Geología Petrolera de México, 1984. *In:* Marmissolle-Daguerre, D., coordinator. Evaluación de Formaciones en México: México, D.F., Schlumberger Offshore Services-PEMEX, p. 1-36.

Rubén Darío Arizabalo[1], Klavdia Oleschko[2], Gabor Korvin[3], Gerardo Ronquillo[1] and Esteban Cedillo-Pardo[1]

[1] Instituto Mexicano del Petróleo, Eje Central 152, Mexico City, Mexico
Email: rarizaba@imp.mx
[2] Instituto de Geología, Universidad Nacional Autónoma de México, Mexico
[3] King Fahd University, Saudi Arabia